

Fermi energy engineering of enhanced plasticity in high-entropy carbides

Kenneth Vecchio ^{a,*}, Stefano Curtarolo ^{b,*}, Kevin Kaufmann ^{a,1}, Tyler J. Harrington ^{a,2},
 Corey Oses ^b, Cormac Toher ^b

^a Department of NanoEngineering, University of California San Diego, La Jolla, CA, 92093, USA

^b Department of Mechanical Engineering and Materials Science, Center for Extreme Materials, Duke University, Durham, NC, 27708, USA

ARTICLE INFO

Keywords:
 Fermi energy
 Enhanced toughness
 High entropy carbides
 Mechanical properties

ABSTRACT

Mechanical properties of a range of high-entropy rocksalt carbides are investigated via *ab-initio* modeling and experimental verification. It is found that elastic constants, hardness, and fracture resistance depend on the electronic structure of the system, which is parameterized through two descriptors: the valence electron concentration (VEC) and the integrated density of states from the pseudo-gap energy to the Fermi energy ($iDOS(E_{pg}, E_F)$). Compositions incorporating more electrons (increasing VEC) shift E_F further above E_{pg} , filling more deformable metal *d*-derived t_{2g} bonding orbitals. MoNbTiVWC₅, MoNbTaVWC₅, CrMoNbVWC₅, and CrMo-TaVWC₅ – stabilizing as a single-phase rocksalt solid solution – each have a VEC ≥ 9.0 , an $iDOS(E_{pg}, E_F) > 5.75$ states/cell, and a higher electron abundance than any of the rocksalt binary and ternary carbides. The materials approach the ductility range, achieving an attractive combination of fracture resistance (i.e. enhanced plasticity) and hardness rarely found in ceramic materials. Entropy, allowing high VEC values to be reached within cubic structures, enables a new path for tailoring mechanical properties.

1. Introduction

The B1 (rocksalt) monocarbides of group IVB, VB, and VIB transition metals have high hardness and elastic modulus, good oxidation/corrosion resistance, and some of the highest melting temperatures of any materials, making them a standard for applications in extreme environments, such as reactor linings, hypersonic vehicle nose tips and wing leading edges, propulsion motor components, bearing materials, electrodes in gas-tungsten/plasma arc welding and arcjet thrusters, furnace elements, and cutting tools [1–3]. When designing for such conditions, mechanical properties are critical. Like other hard materials, transition metal carbides (TMCs) demonstrate little to no plastic flow and lack any dislocation mechanism to dissipate stress at low temperatures, leading to brittle fracture failure [4,5]. Traditionally, increasing fracture toughness of brittle materials has only been done through classical toughening mechanisms, such as fiber bridging, transformation toughening, grain bridging, crack deflection, and ductile phase toughening [6–11]. It has been shown, however, that the TMCs have tailorabile mechanical, thermomechanical, and thermophysical properties based on their electronic structure [1,12,13]. Studies including carbides,

nitrides, and carbonitrides have: i. demonstrated that, although all can be considered highly brittle materials with the rocksalt structure, trends of increasing toughness with valence electron concentration (VEC) are observed, and ii. argued that, since the Peierls stresses are so high (2–3 orders of magnitude higher than metals [14,15]), hardness may depend more on the difficulty of nucleating/moving dislocations in the lattice than on the activation energy to move them through microstructural features [16,17]. Toughness, hardness, and more generally mechanical properties are thus not only tunable through traditional microstructural engineering (Hall-Petch [18], work/precipitate strengthening [19,20]), but also through chemistry/bonding (compositional control and alloying), making multicomponent systems a key area of interest [21].

Most previous studies have focused on the carbon stoichiometry to tailor the mechanical properties of binary carbides, although some recent work has been done on systems including two or more transition metals [13,22,23]. Even among the binary carbides, the choice of the alloying element can have targeted effects on the mechanical properties. For example, HfC and TaC are both stable in the B1 structure and have similar bonding enthalpies (evidenced by their similar ultra-high melting temperatures), yet HfC is brittle when deformed at room

* Corresponding authors.

E-mail addresses: kvecchio@ucsd.edu (K. Vecchio), stefano@duke.edu (S. Curtarolo).

¹ Present address: Oerlikon, San Diego, CA 92127, United States

² Present address: Apple Inc., Cupertino, CA 95014. United States

temperature, while TaC allows for significant plasticity via dislocations [24]. The difference in electronic structure between hafnium and tantalum has two effects on the mechanical response: i. the additional electrons in TaC enhance the overall metallic character of the bonds yielding greater ductility, and ii. the existence of an intrinsic stacking fault causes different active slip systems – the primary slip system in tantalum carbide is $\{111\}\langle110\rangle$, while in the rest of the rocksalt carbides the primary system is $\{110\}\langle1\bar{1}0\rangle$ [12,24,25]. The availability of slip systems, without thermal activation, promotes ductile failure and gives TaC the highest room temperature toughness of any rocksalt TMC [26].

Bonding (stiffening) and defects have also been shown to be two hardening approaches associated with VEC [27–30]. i. Jhi et al. [16] identified peak hardness in carbonitrides at a VEC of 8.4, attributed to the complete filling of the shear resistant $pd\sigma$ bonding states between the metal $d_{x^2-y^2}$ orbitals and the carbon p_x and p_y orbitals. Once the electron population exceeds a VEC of 8.4, metallic character develops, and the much more deformable metal t_{2g} -derived states dominate the density of states. ii. Hugosson et al. [5,31] consider that a VEC $\gtrsim 10$ brings the energies of the cubic and hexagonal polymorph structures in carbides and nitrides closer together. The energetic proximity of competing phases with different stacking sequences facilitates formation of hexagonal stacking faults that enhance hardness by hindering dislocation motion across faults, while also improving ductility (and toughness) by promoting $\{111\}<110>$ slip along the faults [32]. Since the nitrides are inherently more electron rich than the carbides, investigations into enhancing ductility and toughness focus on nitrides, as binary monocarbides are only stable in the B1 configuration up to a VEC of 9.0.

However, VEC alone cannot capture critical electronic features [12, 13, 16, 27–30, 33, 34]. For instance, TaC and NbC have the same VEC, yet only TaC can slip along the $\{111\}$ planes at room temperature, as it possesses an intrinsic stacking fault [12]. Sangiovanni et al. [4,28,30,33] found that while ductility and, therefore, toughness generally increase with VEC in carbides and nitrides, several factors also contribute. They include anion and cation occupation of lattice sites [35–37], competition between different polymorph structures (in B1 solid solutions) of parent binary phases [5,31,32], effects of the degree of cation-sublattice ordering [38–40] and solid-solution strengthening [41] (due to internal residual stresses and composition modulation), energetically-favored formation of extended defects (e.g. stacking faults [5,31,32]) and strain-induced structural transformations [25,42], and non-linear elastic effects [43].

To capture the mechanism beyond VEC, Das et al. [44] compared the DOS of the transition metal carbides of Sc, Ti, V, Zr and Hf. Each TMC demonstrates a characteristic bonding/anti-bonding structure with a pseudo-gap arising from the dominating covalent-like bonding between the transition metal t_{2g} -orbitals and the C p -orbitals [44,45]. The Fermi energy (E_F) lies i. below the pseudo-gap, for the group IIIB metal (Sc), ii. directly in the center of the pseudo-gap for the group IVB metals (Zr, Ti, Hf), and iii. above the pseudo-gap for the group VB metals (V) [44]. Das et al. [44] also stated that for TiC and ZrC, strong bonding can be expected because E_F sits at the center of the pseudo-gap where the DOS is low; the TMCs of group IV metals indeed have the highest hardness values [16,27]. In more complex alloy systems, through selection of alloying elements, the relationship between the pseudo-gap and E_F can be tuned, allowing control over mechanical properties.

Hypothetically, if a carbide can be stabilized in the rocksalt structure at room temperature having a VEC higher than 9.0, it would exhibit greater plasticity and fracture toughness than the binary TMCs, which can be demonstrated in calculation of mechanical properties of rocksalt structured WC and MoC. Theoretical works investigating alloys of group VIB transition metals (i.e., W and Mo) with group VB TMCs have demonstrated that these materials should indeed exhibit significantly enhanced plasticity [4]. However, experimentally, alloys of WC and MoC are only stable in the rocksalt structure at elevated temperatures

(stabilized dynamically by lattice vibrations at finite temperatures) [46–51], when alloyed with other transition metal carbides (e.g., vanadium carbide) [23], or for low concentrations of Mo and W at low temperatures. Opportunities to optimize VEC and combine properties of interest, such as hardness and toughness, exist by alloying. In particular, “extreme” alloying, i.e. high entropy, promotes solubilities significantly while also inherently enhancing hardness, oxidation/corrosion resistance, and thermodynamic stability [21]. High-entropy carbides (HECs) containing a high atomic fraction (10 at% each) of combinations of Cr, Mo, and W, and forming a single phase rocksalt structure at the atomic scale, were recently synthesized [52–55]. In particular, the synthesis of the equiatomic high-entropy compounds MoNbTiVWC_5 , MoNbTaVWC_5 , CrMoNbVWC_5 , and CrMoTaVWC_5 show a single, randomly ordered rocksalt phase with a VEC > 9.0 , surpassing the conventional limit for binary monocarbides stable in the B1 configuration. While there is no a-priori reason to disfavor other possible organizations, rock-salt is the most obvious structure, as high-entropy equiatomic solid-solutions of transition-metal mono-carbides have so far appeared only in rock-salt structures, even if some of the constituents’ carbides are not cubic [21]. This also compounds with the fact that high-entropy tends to stabilize simple structures which has been seen for both high-entropy metallic alloys and ceramics [79]. An analysis of the whole phase diagram with associated heat of formation to determine the entropy promotion gain versus the enthalpy loss at the onset of the order/disorder transition was recently performed by Divilov et al. [80] using the “disorder enthalpy-entropy descriptor” (DEED) formalism”. In this work, no high-entropy carbide and carbonitride was experimentally synthesized having a structure different than rock-salt.

In this article, we explore the tunability of mechanical properties in high-entropy carbides through control of composition, which determines electronic structure. We relate the elastic constants, hardness, and fracture toughness to the electronic structure through the VEC and the integrated density of states (iDOS) from the pseudo-gap energy to the Fermi energy ($iDOS(E_{pg}, E_F)$) – an effective metallicity descriptor. This theory allows for precise tunability of mechanical properties and, through entropic promotion, the development of stable HECs with high hardness and fracture toughness.

2. Experimental

2.1. AFLOW for high-entropy alloys

The representative ordered configurations, called *tiles*, required to calculate the energy spectrum are generated using the AFLOW-POCC algorithm [56] implemented within the AFLOW computational materials design framework [57,58]. The algorithm initially constructs superlattices of the minimum size necessary to obtain the nominal stoichiometries to within some user-specified accuracy. For each unique superlattice, the AFLOW-POCC algorithm then generates the complete set of possible supercells using Hermite normal form matrices. Non-unique supercell combinations are eliminated from the ensemble by first estimating the total energies of all configurations using a Universal Force Field-based method [59], and then identifying duplicates from their identical energies.

For structure generation in the case of the high-entropy carbide systems investigated here, the AFLOW-POCC algorithm starts with the rock-salt crystal structure (space group: $Fm\bar{3}m$, #225; Pearson symbol: cF8; AFLOW Prototype: AB_cF8_225_a_b [60]) as the input parent lattice. Each anion site is occupied with a C atom (occupancy probability of 1.0), while the cation site is occupied by 5 different refractory metal elements, with a 0.2 occupancy probability for each. The AFLOW-POCC algorithm then generates a set of configurations (600 in total, 49 unique in the case of the rock-salt based 5-metal carbide systems), each containing 10 atoms: one atom of each of the metals, along with 5 carbon atoms. This is the minimum cell size necessary to accurately reproduce the required

stoichiometry.

The properties for the disordered structure are calculated with a Boltzmann-weighted average (at 2200°C or 2473 K: the experimental sintering temperature) of the 49 representative ordered structures ensemble. The DOS is first calculated for each ordered structure with AFLOW, which leverages VASP using parameters defined by the AFLOW Standard [61]. AFLOW-POCC then resolves the ensemble-average DOS, from which the iDOS(E_{pg} , E_F) can be determined: E_F is the Fermi energy and E_{pg} is taken as the energy of the minimum value of the total density of states near E_F .

The algorithm could consider larger cells, e.g. 20-atom cells, of which there are 2,041,200 possible configurations with about 69,285 unique – beyond computational capabilities even for a single system. Whether larger cells are needed depends on the correlation lengths of the structure/property in consideration. The 10-atom cell models the local environment to within at least second nearest neighbors ($M-C$ and $M-M$, etc.). Early EXAFS spectra for 5-metal high-entropy oxides suggests that these are the most important interactions to capture for these materials [62].

2.2. Calculating elastic constants

Elastic properties, including the elastic constants and moduli, are calculated using the Automatic Elasticity Library (AEL) module [63] of the AFLOW framework, which applies a set of independent directional normal and shear strains to the structure, and fits the resulting stress tensors to obtain the elastic constants. From this, the bulk (B) and shear (G) moduli are calculated in the Voigt, Reuss, and Voigt-Reuss-Hill (VRH) approximations, with the VRH average being used for the purposes of this work.

The elastic properties for the 5-metal compositions are first calculated for each of the 49 configurations generated by AFLOW-POCC. The average elastic constants and moduli are then obtained and weighted, according to the Boltzmann distribution, at a temperature of 2200°C (2473 K, the experimental sintering temperature).

Ductility is modeled using the Pugh's modulus ratio ($k = G/B$) and the Cauchy pressure ($C_{12} - C_{44}$). Since the disordered materials do not have cubic symmetry, the difference between averaged values of the elastic constants $(C_{12} + C_{13} + C_{23})/3$ and $(C_{44} + C_{55} + C_{66})/3$ is used to calculate the Cauchy pressure [4,64]. Three different models are used for predicting the Vickers hardness based on the elastic moduli:

Chen et al. [65]

$$\left(H_V = 2(k^2 G)^{0.585} - 3 \text{ where } k = \frac{G}{B} \right),$$

Teter [66]

$$(H_V = 0.151G)$$

and Tian et al. [67]

$$(H_V = 0.92k^{1.137}G^{0.708}).$$

Note, however, that these models are based on the elastic response of the materials, and do not consider excitations of internal modes (phonons) or phenomena such as plastic deformation, slip planes, and lattice and bulk defects. These models have been shown to offer good qualitative agreement for superhard materials [68], including ceramics [53, 69]. The reported value for calculated hardness is the average H_V calculated using the three different techniques.

2.3. Synthesis

Each of the carbide compositions is weighed out in 24 g batches using binary carbide powders (TiC, ZrC, HfC, VC, NbC, TaC, Cr₃C₂, Mo₂C, WC, C; Alfa Aesar, USA). Powders are hand mixed and high energy ball milled in a shaker pot ball mill for a total of 2 h in 30-minute increments,

intersected by 10-minute rests to avoid overheating. Samples are sintered using current and pressure assisted densification (CAPAD), also known as spark plasma sintering or field assisted sintering technique, in a vacuum environment. The temperature and pressure profile for each sample is as follows: heat to 2200°C at 100°C/min under 5 MPa uniaxial load; hold for 9 min; increase load to 80 MPa at 75 MPa/min while at 2200°C; hold for 15 min; cool under ambient conditions. The initial vacuum is less than 20 mTorr prior to heating. Whenever the vacuum exceeds 100 mTorr, the heating and pressure profile is held until the vacuum again reaches less than 20 mTorr. All sintering is done in graphite die and plunger sets. Each sample is ground and polished to 0.04 μm colloidal silica on both sides to remove any remaining carbon.

2.4. Experimental elastic constants from acoustic wave speed

All moduli are obtained following ASTM standard E494–15. Sample dimensions are on average 20 mm diameter and 3 mm in height cylindrical pucks. Both sides of samples are ground and polished, and then placed on an acoustically isolated substrate to ensure no interference from the local surroundings. Using a piezoelectric transducer coupled with an oscilloscope, the reverberating sound waves are measured and recorded. For each sample, a total of four longitudinal and four shear waves at different intervals are recorded in order to calculate the respective velocities. After determination of the velocities, Poisson's ratio (ν), Young's modulus (E), shear modulus (G), and bulk modulus (B) are determined using Eqs. (1–4) below:

$$\nu = \frac{V_L^2 - 2V_S^2}{2(V_L^2 - V_S^2)}, \quad (1)$$

$$E = 2V_S^2\rho(1+\nu), \quad (2)$$

$$G = \rho(V_S^2), \quad (3)$$

and

$$B = \frac{E}{3(1-2\nu)}, \quad (4)$$

where ρ is the density, V_L the longitudinal wave velocity, and V_S the shear wave velocity.

2.5. Hardness and fracture toughness from indentation

Samples are polished and mounted in preparation for Vickers microhardness following ASTM standard E92–17. A Leco micro-indentor is used to create indents in each sample. A total of 20 indents with an applied load of 0.98 N (100 gf) are done on each sample, and their location subsequently marked on the sample. After indentation, the samples are then loaded into a Thermo-Fisher (formerly FEI) Apreo scanning electron microscope, the indents are individually imaged, and the size of the indents measured. The Vickers hardness (H_V) values are determined using the cross-diagonal measurements obtained from SEM imaging via Eq. (5) below:

$$H_V = \frac{P}{d_1 d_2}, \quad (5)$$

where P is the load force in N, d_1 the horizontal diagonal, and d_2 the vertical diagonal.

Fracture toughness is calculated according to the methods laid out by Anstis et al. [70]. Crack lengths are measured simultaneously upon measuring the hardness values of each individual indent. Criteria for viable indents are as follows: cracks measured must be propagating from the corners of the indent, the indent must be uniform and in accordance with ASTM standards for hardness calculation, crack paths must be devoid of obstructions, such as pores in the sample. After obtaining

crack lengths, fracture toughness is computed via Eq. (6) below [70]:

$$K_{ifr} = 0.016 \left(\frac{E}{H_V} \right)^{\frac{1}{2}} \frac{P}{c^{\frac{3}{2}}} \quad (6)$$

where E and H_V are in units of GPa, P is the load force in N, and c is the crack length from the center of the indent in units of meters. Fracture toughness values are determined using H_V and c for each individual indent and the final reported K_{ifr} is taken as the average across all viable indents (minimum of 10) for a given sample.

3. Results

3.1. Modeling

The primary hypothesis of this work is that if carbides having a VEC greater than 9.0 can be stabilized in the rocksalt structure at room temperature, these materials would exhibit greater plasticity and fracture toughness than carbides with a VEC less than or equal to 9.0. The basis for this hypothesis is demonstrated via calculation of mechanical properties of the theoretical rocksalt structured WC and MoC both having a VEC of 10.0 (Fig. 1). The list of nine HEC compositions chosen in this work are given in Table 1 along with their calculated VEC, iDOS (E_{pg} , E_F), and DOS(E_F). Compositions were chosen to provide a spread of HECs ranging from low to high electron population at regular intervals (i.e., seven 0.2 VEC steps) with two compositions represented for VEC =

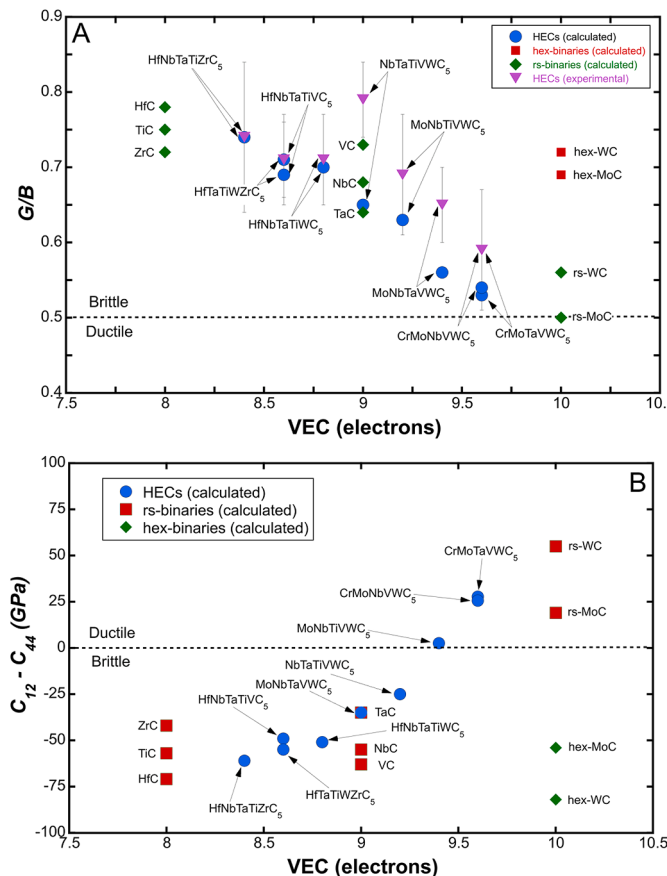


Fig. 1. (A) The modeled and experimental Pugh's Modulus ratio (G/B) for each of the HECs along with the calculated values for the rocksalt (rs) binary carbides and hexagonal (hex) binary carbides and (B) the calculated Cauchy pressures for each of the HECs and rs and hex binary carbides. Note that the lowest Pugh's modulus ratio and highest Cauchy pressure is attained with MoNbTaVWC_5 when considering that rocksalt WC and MoC are not stable at room temperature.

Table 1

List of compositions and corresponding valence electron concentration (VEC), Fermi energy ductility parameter (iDOS(E_{pg} , E_F)) and electronic density of states at the Fermi energy (DOS(E_F)) taken from density functional theory.

Composition	VEC	iDOS(E_{pg} , E_F) (states/cell)	DOS(E_F) (states/eV)
HfNbTaTiZrC_5	8.4	2.29	2.88
HfNbTaTiVC_5	8.6	3.53	3.85
HfTaTiWZrC_5	8.6	3.41	3.06
HfNbTaTiWC_5	8.8	4.40	3.00
NbTaTiVWC_5	9	5.75	4.56
MoNbTiVWC_5	9.2	6.14	4.90
MoNbTaVWC_5	9.4	7.66	5.09
CrMoNbVWC_5	9.6	8.00	5.94
CrMoTaVWC_5	9.6	8.03	5.68

8.6 and VEC = 9.6 and four compositions with VEC > 9.0. The lowest valence electron density composition, consisting of three group IVB and two group VB transition metals is HfNbTaTiZrC_5 , while the highest, comprising three group VIB and two group VB are the compositions CrMoNbVWC_5 , and CrMoTaVWC_5 . The total spread of VEC ranges from 8.4 to 9.6. The full electronic density of states, from which the iDOS(E_{pg} , E_F) was determined for each of the carbide compositions, are shown in Fig. 2. The electronic density of states for each of the HECs shows a pseudo-gap, which is characteristic of rocksalt transition metal carbides [44]. All of the compositions investigated have E_F greater than the pseudo-gap energy (E_{pg}). The distance between E_F and E_{pg} becomes larger as E_F shifts to higher energies, indicating filling of metallic d -derived t_{2g} states and an effective increase in the metallic character of the bonding. Hybridization of the $s/p/d$ orbitals can be ruled out as the dispersion of s - and p -states is quite constant and not associated to any onset of d -peaks. We conclude that the extra charge injected by tailoring the composition ends up in t_{2g} states and interstitial delocalized positions, typical of metals.

There is a near-linear correlation between the VEC and the iDOS(E_{pg} , E_F) with a Pearson correlation coefficient of 0.99 (see Fig. 3), suggesting that the parameter iDOS(E_{pg} , E_F) may function as a successful descriptor of bonding metallicity, as well as a better parameter on which to base engineering of mechanical properties than the DOS(E_F). The iDOS incorporates both the absolute value of the density of states at E_F and the distance between the pseudo-gap and E_F , which describes the number of metal d -derived t_{2g} states available for electron population more effectively than simply DOS(E_F). Further, the VEC may be an oversimplification of electronic structure and, therefore, may not capture subtle differences that will be resolved by iDOS(E_{pg} , E_F). For example, HfTaTiWZrC_5 and HfNbTaTiVC_5 both have a VEC of 8.6; however, they have an iDOS(E_{pg} , E_F) of 3.41 and 3.53 states/cell, respectively.

Fig. 4(A-C) show the correlation between iDOS(E_{pg} , E_F) and the calculated elastic properties from DFT. The integrated density of states and bulk modulus have a positive Pearson (linear) coefficient of 0.88. The iDOS correlates more strongly with the calculated modulus than either the VEC (Pearson = 0.84) or the DOS(E_F) (Pearson = 0.78), corroborating that the iDOS most effectively describes the nature of the bonding as it relates to mechanical properties. For increasing iDOS(E_{pg} , E_F), the shear and elastic moduli first increase and then steadily reduce, in agreement with previous theoretical work on binary carbides and nitrides [27] and previous results in high-entropy carbides [52]. The maximum for shear modulus is near a VEC of 9 (the maximum available for any binary rocksalt carbide) or iDOS(E_{pg} , E_F) equal to 4.40 states/cell (the value for HfNbTaTiWC_5). The decreasing shear modulus at high electron concentrations is an important factor when considering ductility or toughness in high-entropy carbides (HECs).

In order to predict the brittle or ductile behavior of any material composition using elastic constants, the simple formulation of Pugh [71] can be applied, where the plastic properties of metals are linked to their elastic moduli [4,27,72]. In general, if the ratio of shear modulus to bulk modulus is less than 0.5 ($G/B < 0.5$), the material will behave in a

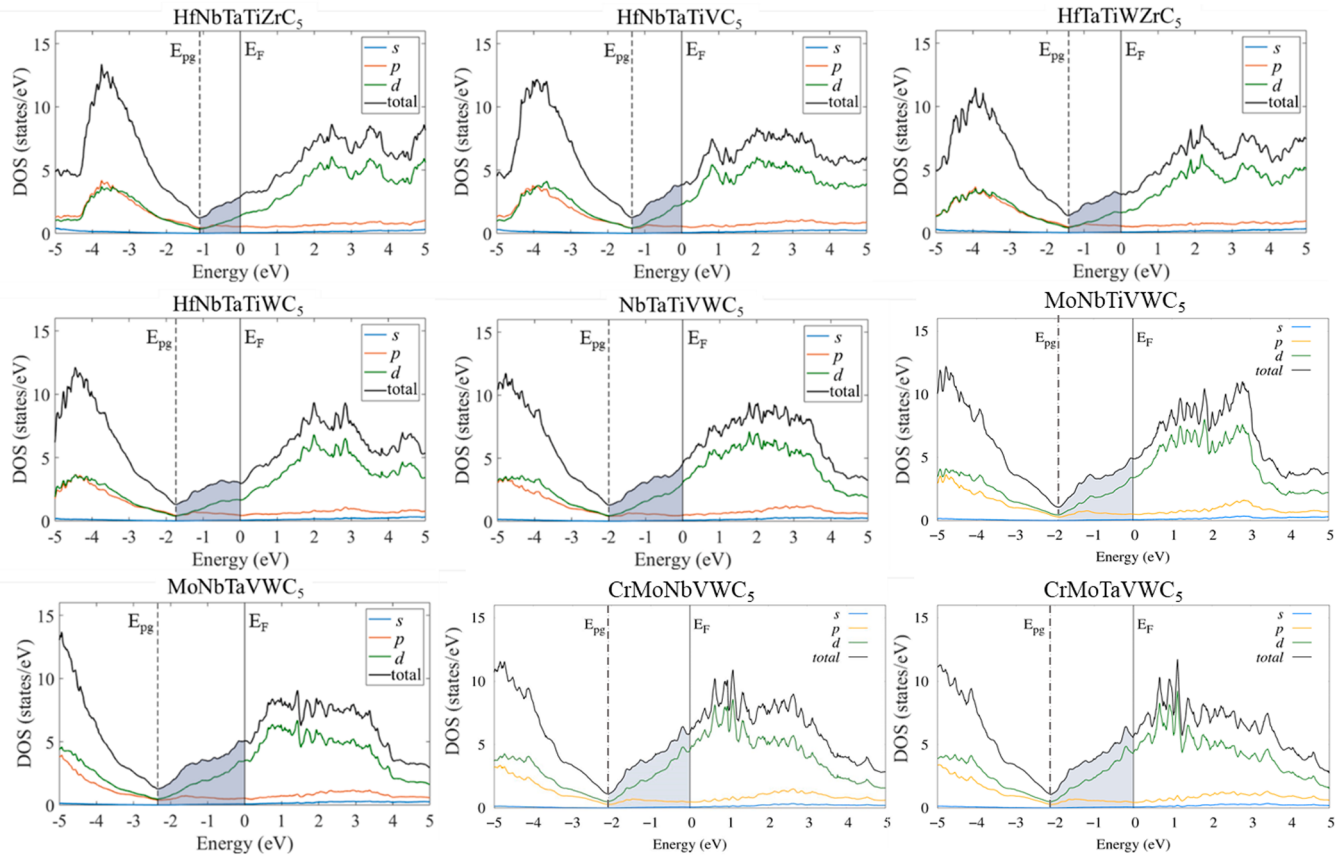


Fig. 2. Complete electronic density of states for each of the high-entropy carbide compositions. The pseudo-gap energy (E_{pg}) and Fermi energy (E_F) are indicated by dashed and solid vertical lines, respectively. The shaded region represents the iDOS(E_{pg}, E_F) for each composition.

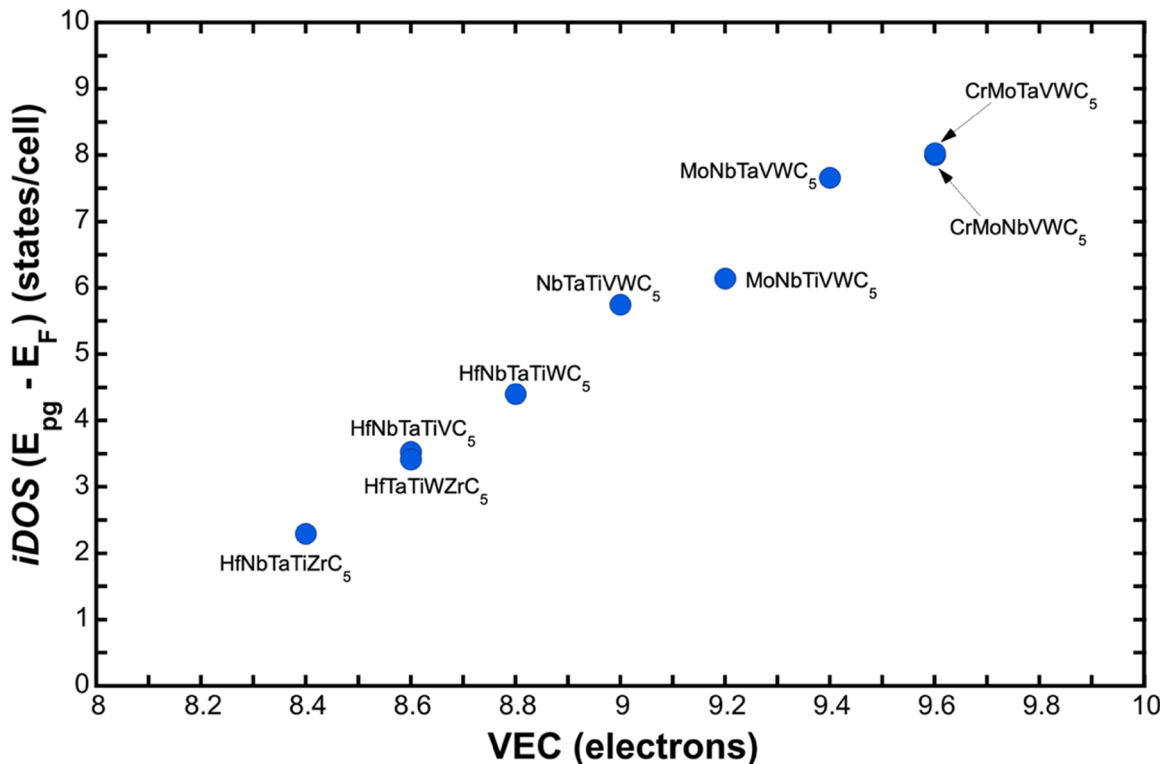


Fig. 3. The integrated density of states from the pseudo-gap energy to the Fermi energy (iDOS(E_{pg}, E_F)) against the VEC for nine solid solution high-entropy carbide compositions. The iDOS increases linearly with VEC with a Pearson (linear) correlation coefficient of 0.99.

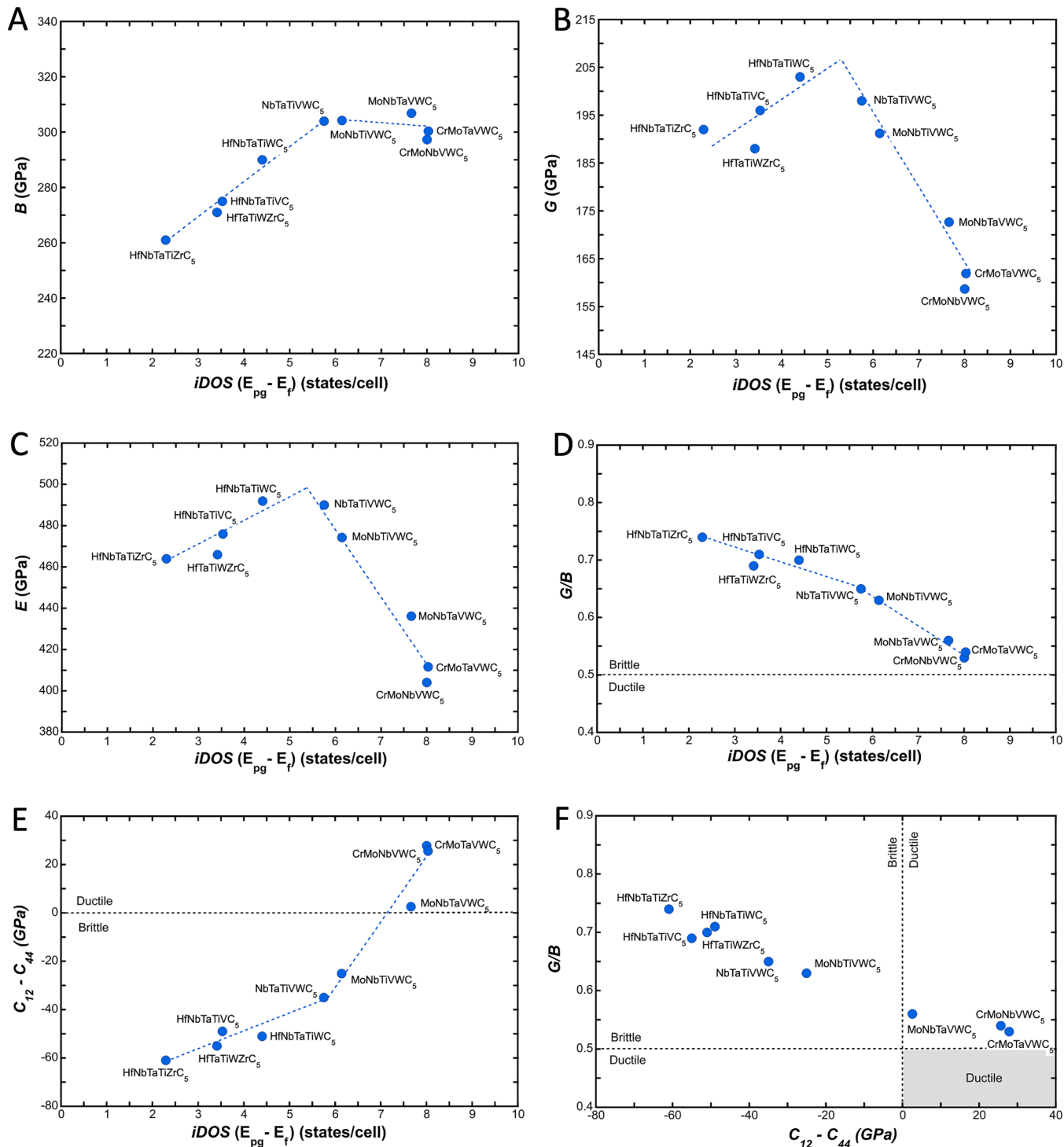


Fig. 4. Calculated moduli and ductility parameters of high-entropy carbides. (A-C) DFT predicted bulk (B), shear (G), and elastic (E) modulus against $iDOS(E_{pg}, E_f)$ for each of the HEC compositions and (D) the relationship between predicted Pugh's modulus ratio (G/B) and $iDOS(E_{pg}, E_f)$, (E) the relationship between Cauchy pressure ($C_{12} - C_{44}$) and $iDOS(E_{pg}, E_f)$ and (F) calculated Pugh's modulus ratio and Cauchy pressure for each of the six HEC compositions, which tend towards the ductile regions with increasing electronic population. A ductile material would have a Pugh's modulus ratio below 0.5 and a positive Cauchy pressure, indicated by the shaded region in the bottom right corner of the plot. Trend lines are 1) a linear fit to the data from $iDOS(E_{pg}, E_f)$ of 2.29–4.40 states/cell (first four data points) and 2) a linear fit to the data from $iDOS(E_{pg}, E_f)$ of 4.40–8.03 states/cell (last five data points).

ductile manner, otherwise it will be brittle [71,72]. Thus, the establishment of a relationship between the moduli and a relevant electronic parameter, such as the $iDOS(E_{pg}, E_f)$, can help to tune the ductility of HECs based on compositional control of alloying elements, which can be easily chosen to have specific effects on the $iDOS(E_{pg}, E_f)$. The Pugh's modulus ratio (G/B) and the parameter $iDOS(E_{pg}, E_f)$ (plotted in Fig. 4D)

have a strongly negative Pearson correlation of -0.98 . Thus, as the elements used in alloying HECs move the overall composition to a more valence-electron-rich region, the system becomes more ductile. Note that since G reaches a maximum around 4.40 states/cell while B continues to increase, G/B decreases more quickly above this value. MoNbTaVWC₅, CrMoNbVWC₅, and CrMoTaVWC₅ have the lowest predicted

Pugh's modulus ratio of 0.53 to 0.56 (close to 0.5) and should, therefore, most effectively promote slip under an applied stress, leading to a higher fracture toughness. Since G/B is above 0.5, MoNbTaVWC₅, CrMoNbVWC₅, and CrMoTaVWC₅ are not expected to behave as a

ductile (metallic) material, but should accommodate more plasticity, which should manifest on the macroscale as enhanced toughness.

A second method of determining ductility from predicted elastic parameters is the formulation of Pettifor [73], developed for

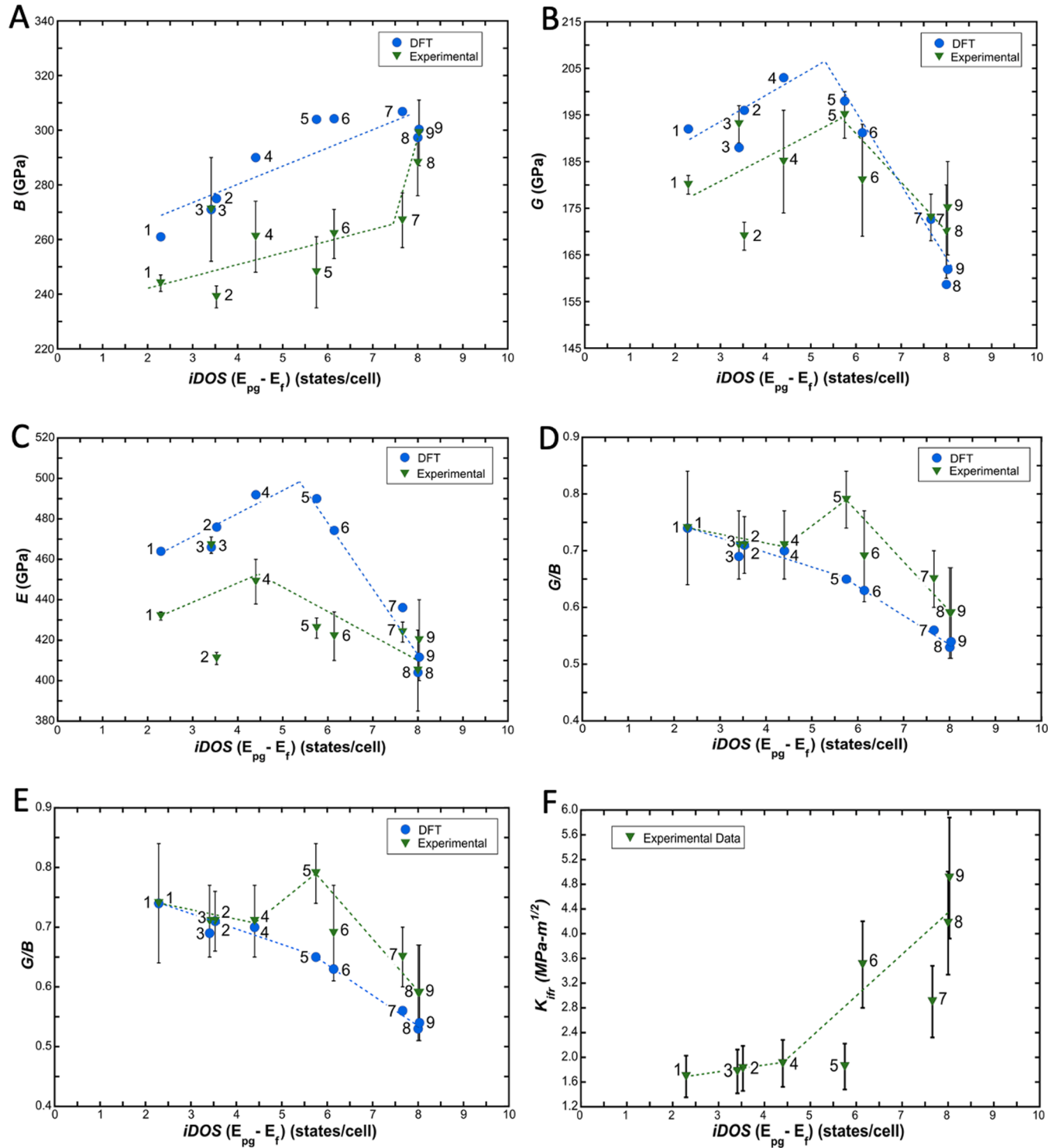


Fig. 5. Experimental moduli and mechanical properties of high-entropy carbides. Predicted and experimental (A) bulk moduli, (B) shear moduli, (C) elastic moduli, (D) Pugh's modulus ratios, (E) Vickers hardness, H_V , and (F) experimental indentation fracture toughness, K_{ifr} , against the $iDOS(E_{pg}, E_f)$ metallicity descriptor for each of the six high-entropy carbide compositions. Reported errors are ± 1 standard deviation from measurements on a minimum of 10 indentations satisfying the conditions for fracture toughness outlined in Methods. Individual composition labels are left off for clarity in showing trends, however the compositions are: 1. HfNbTaTiZrC₅, 2. HfNbTaTiVC₅, 3. HfNbTaTiWC₅, 4. HfTaTiWZrC₅, 5. NbTaTiVWC₅, 6. MoNbTiVWC₅, 7. MoNbTaVWC₅, 8. CrMoNbVWC₅, and 9. CrMo-TaVWC₅. Trend lines are 1) a linear fit to the data from $iDOS(E_{pg}, E_f)$ of 2.29–4.40 states/cell (first four data points) and 2) a linear fit to the data from $iDOS(E_{pg}, E_f)$ of 4.40–8.03 states/cell (last five data points).

intermetallic systems, in which the angular character of bonding can be used to determine mechanical properties. Since the Cauchy pressure is defined as $C_{12} - C_{44}$ (where C_{12} and C_{44} are components of the stiffness tensor), if the bonding is simple pair-wise potentials, then the Cauchy pressure will be zero [74]. If the Cauchy pressure is negative, then the bonding is more angular, and the orbitals will resist deformation in response to stress (i.e. brittle) [73]. If the bonding is more metallic and hence less directional, then the Cauchy pressure will be positive. Thus, a positive Cauchy pressure denotes a more metallic and, therefore, more ductile material. Fig. 4E shows the Cauchy pressure ($C_{12} - C_{44}$) against the iDOS(E_{pg}, E_F) parameter. The Cauchy pressure scales with iDOS(E_{pg}, E_F) with a high Pearson coefficient of 0.95. As with the Pugh's modulus ratio, the Cauchy pressure shows a more drastic rate of increase when the iDOS(E_{pg}, E_F) is greater than 4.40 states/cell and are notably positive for MoNbTaVWC₅, CrMoNbVWC₅, and CrMoTaVWC₅. These trends suggest that with the use of entropy promotion, which allows for stable rocksalt compositions containing group VIB metals, even more significant enhancements in ductility can be achieved than when moving from group IVB to VB binary carbides. Fig. 4F presents a plot of Pugh's modulus ratio against Cauchy pressure, common in determination of material ductility from predicted elastic properties [4]. Here, the most ductile materials should fall in the bottom right corner of the plot and the compositions MoNbTaVWC₅, CrMoNbVWC₅, and CrMoTaVWC₅ are again the closest to that region with a positive Cauchy pressure and G/B close to 0.5, which almost satisfies the ductility parameters put forth by Pettifor [73]. To predict the mechanical properties of the HECs, a comparison is made between the calculated Pugh's modulus ratio, the Cauchy pressure, and the VEC of the HECs, the rocksalt binary carbides of group IVB and VB transition metals, and rocksalt and hexagonal binary carbides of group VIB transition metals (Fig. 1).

Note that WC and MoC in the rocksalt structure fall well into the ductile region for both ductility criteria, but the hexagonal WC and MoC lie firmly within the brittle region. Since these binaries are only stable as rocksalts at high temperatures [2], the most ductile material, even when considering all of the rocksalt binaries, should be the high-entropy compositions MoNbTaVWC₅, the one with both the highest entropy forming ability and the highest activation enthalpy in the original discovery study of Sarker et al. [53], along with the two compositions containing Cr, Mo, and W (CrMoNbVWC₅ and CrMoTaVWC₅) discovered by Kaufmann et al. [54].

3.2. Experimental mechanical properties

For experimental verification of predicted properties, each of the HECs was synthesized in bulk form. Fig. 5 shows the trend of measured bulk moduli (Fig. 5A), shear moduli (Fig. 5B), elastic moduli (Fig. 5C), and Pugh's modulus ratios (Fig. 5D) against the iDOS(E_{pg}, E_F) parameter. The moduli are in good agreement with the predicted values from DFT and demonstrate the expected relationships with increasing available electron states. All of the moduli show slight negative deviations from predicted values, which is likely due to sample imperfections such as porosity, impurities, and oxide inclusions. There is some cancellation of the deviations when calculating the Pugh's modulus ratio, so the ductility criteria agree well with predicted values. By Pugh's criteria, the compositions with the highest iDOS(E_{pg}, E_F) – CrMoNbVWC₅ and CrMoTaVWC₅ – should be the most ductile.

In order to design a high-toughness material, the ideal composition would have both high hardness and ductility. The experimental and calculated Vickers hardness for each of the HEC compositions are shown in Fig. 5E. Most of the measured hardness values are lower than that calculated from DFT, which, as with the moduli, is likely due to imperfections (mainly porosity) in the sintered experimental samples. Further, the models for predicting hardness are based on the elastic response of the materials, and do not consider phenomena, such as plastic deformation, slip planes, and lattice and bulk defects. The hardness displays the expected trend of reducing hardness with

increasing iDOS(E_{pg}, E_F), indicating softening of the materials with more electrons and spherical metallic bonding nature. However, the hardness of the most ductile, entropically promoted compositions – CrMoNbVWC₅ and CrMoTaVWC₅ – remains at the relatively high value of 23 GPa, a similar value to the compositions with iDOS(E_{pg}, E_F) between 2.29 and 3.41 states/cell. The high hardness obtained in the HECs coupled with improved plasticity should result in electron-rich compositions forming high-toughness materials. The relatively level hardness trend up to an iDOS(E_{pg}, E_F) of 4.40 states/cell and subsequent decreasing trend should again be noted.

Since the main goal of designing high-entropy carbides that can exhibit significant plasticity is to increase toughness, the indentation fracture toughness, K_{ifr} , of each of the compositions is given against the iDOS(E_{pg}, E_F) in Fig. 5F. As expected, the HECs display enhanced fracture toughness with increasing iDOS(E_{pg}, E_F), indicating that the use of group VIB elements in a high atomic fraction in HECs can effectively strengthen the metallic character of the bonding in the system, improving ductility and fracture toughness. Further, the trend again shows a more drastic rate of increase as the iDOS(E_{pg}, E_F) value exceeds 4.40 states/cell or a VEC of 9.0.

As K_{ifr} increases, the HECs should be able to accommodate increasing plastic deformation before initiation of a crack. The correlation between VEC and fracture resistance was recently demonstrated experimentally during nanoindentation using a range of applied forces and the results summarized by a parameter deemed force-controlled effective fracture resistance (I_{fr}^L) [33]. In brief, I_{fr}^L accounts for the deformation and load induced by an indenter tip when analyzing the percentage of indentation tests for which an alloy does not crack.

Alloys that exhibit a greater percentage of indents that do not manifest cracks with increasing loads will have a higher I_{fr}^L value. The K_{ifr} data for the nine HECs studied herein is overlaid on the I_{fr}^L results from Sangiovanni et al. [33], in which all six of the studied compositions overlap with HECs in this work. Notably, the indentation fracture resistance values measured herein correlate markedly well with whether the material can withstand increased indentation loads without crack formation (I_{fr}^L) and the exponential increase in fracture resistance performance observed in the prior work with VEC increasing above 9.0 (see Fig. 6).

During deformation via indentation, HECs are verified to exhibit plasticity (i.e. dislocations) (Fig. 7). Transmission SEM (t-SEM) of a cross section of a deformation region below an indent made in a sample of HfNbTaTiZrC₅ shows a plastic strain field consisting of extensive dislocation networks, and no visible fractures are apparent. Orientation maps show significant variation, indicating a large change in the crystal

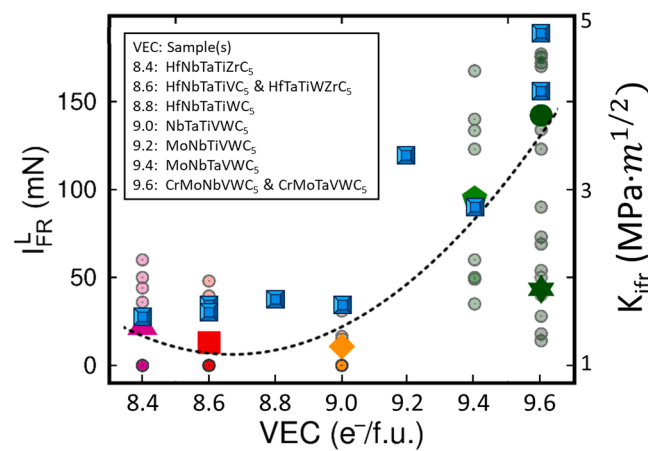


Fig. 6. Indentation fracture toughness compared to effective fracture resistance. The K_{ifr} measurements from the current work (plotted as nine faceted blue squares) are overlaid on the effective fracture resistance measured for six HECs and hypothesized trendline from Sangiovanni et al. [33].

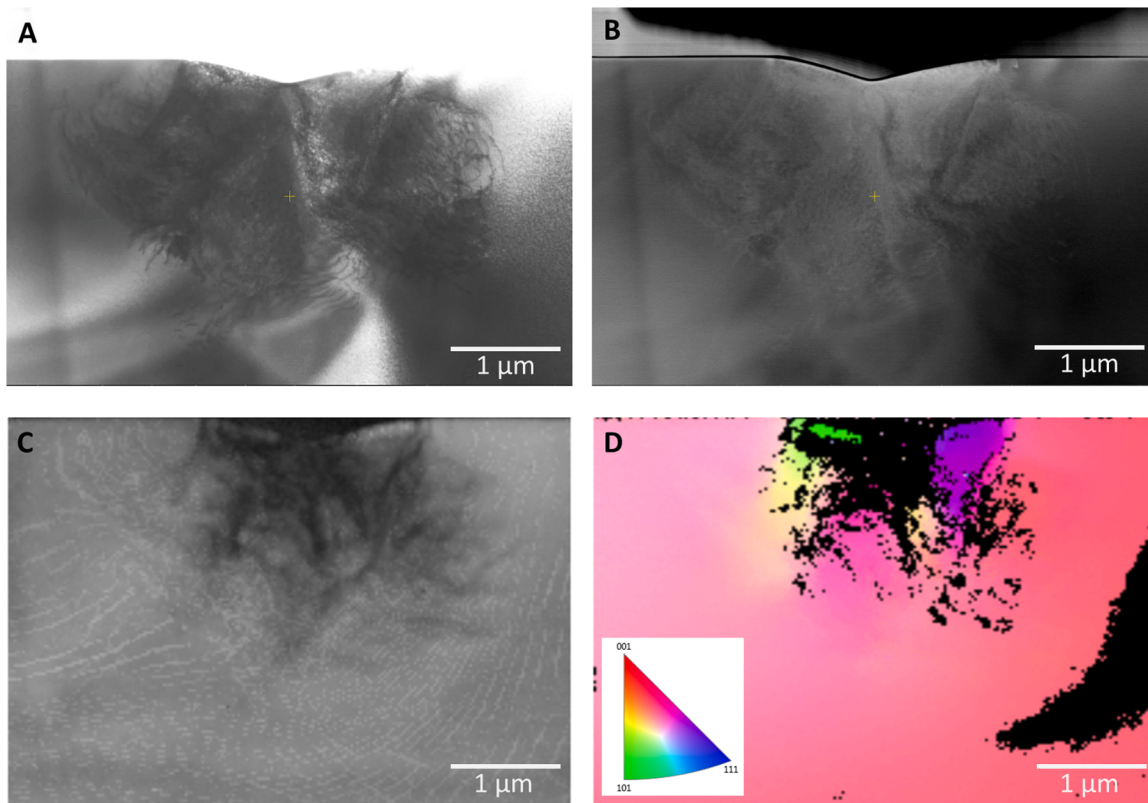


Fig. 7. (A) Transmission SEM (t-SEM) bright field, (B) high angle annular dark field images of a cross section of an indent made in a sample of HfNbTaTiZrC₅ using a Berkovich indenter and 150 mN force and (C) the corresponding band contrast map, and (D) y-direction inverse pole figure map. The y-direction corresponds to the surface normal loading direction in indentation.

rotation tensor and, therefore, accommodation of geometrically necessary dislocations. There exists a decrease in band contrast surrounding the indent edges, which is expected, and indicative of large plastic strain in the lattice that reduces symmetry within the diffracting area and, as a result, decreases the pattern quality and band contrast of the Kikuchi patterns [75].

4. Discussion

4.1. Modeling

The increase in the parameter iDOS(E_{pg} , E_F) directly shows the movement of the Fermi energy (E_F) to higher energies as the transition metal d-states are filled with more electrons. Specifically, the octahedral t_{2g} -derived bonding states of the metals contribute more to the overall density of states, indicating a more metallic bonding character [44]. Thus, the iDOS(E_{pg} , E_F) parameter, which might be referred to as a Fermi energy ductility parameter, is a simple descriptor of metallic character in rocksalt carbides and can be used to predict and tune mechanical properties.

From Pugh's ductility criterion, a high bulk modulus and low shear modulus are desirable to maximize ductility. The bulk modulus scales linearly with iDOS(E_{pg} , E_F), whereas the shear modulus increases up to an iDOS(E_{pg} , E_F) of 4.40 states/cell (or VEC=9.0) and then decreases. This indicates that the improved plasticity in binary carbides with VEC up to 9.0 is more strongly dependent on the bulk modulus trend, rather than the shear modulus. Beyond the group VB transition metals, however, the shear modulus drops, indicating that G/B will fall even faster than for the low VEC materials. The combined effect of the shear modulus decreasing - while bulk modulus continues to increase - is only observed in phase pure, rocksalt systems including significant amounts of elements from group VIB, which is enabled by high-entropy carbides.

The Cauchy pressure also tends to scale with iDOS(E_{pg} , E_F), indicating that the carbides should become more metallic in nature with more electrons. The reduction in angular bonding in the system and strengthening in metallic character should be accompanied by an improvement in plasticity and toughness. Since the Fermi energy ductility parameter iDOS(E_{pg} , E_F) can be used to determine mechanical properties of carbides, a new route to development of ultra-tough materials is presented here. The use of entropic promotion and the exploration of the single-phase high-entropy carbides gives access to a vast new composition space and a resulting new library of electronic density of states that can be searched for parameters such as iDOS(E_{pg} , E_F) in order to find compositions with desirable properties such as hardness and ductility.

4.2. Mechanical properties

It has been well established that the binary carbides demonstrate more significant plasticity as the number of valence electrons in the system increases beyond 8.4. However, the synthesis of rock-salt structure carbides that are more electron rich than TaC remains difficult, since they are more stable in a hexagonal or orthorhombic phase. Here, entropy promotes compositions containing 20 at% of CrC, WC and MoC each (10 at% Cr, 10 at% Mo, 10 at% W), occupying 60 % of the cation lattice, and attaining VEC values of up to 9.6. The randomly ordered solid solution MoNbTaVWC₅ forms a homogeneous single phase through a large temperature range from <700°C to T_m (Fig. 8). The compositions with the most metallic character via VEC and iDOS(E_{pg} , E_F) parameters correspond to the lowest hardness and highest fracture toughness. Although the hardness is less than any of the other HECs, the composition MoNbTaVWC₅ still maintains a high hardness of 19.2 GPa and a high fracture toughness of 2.91 MPa·m^{1/2} compared to TaC, which has an

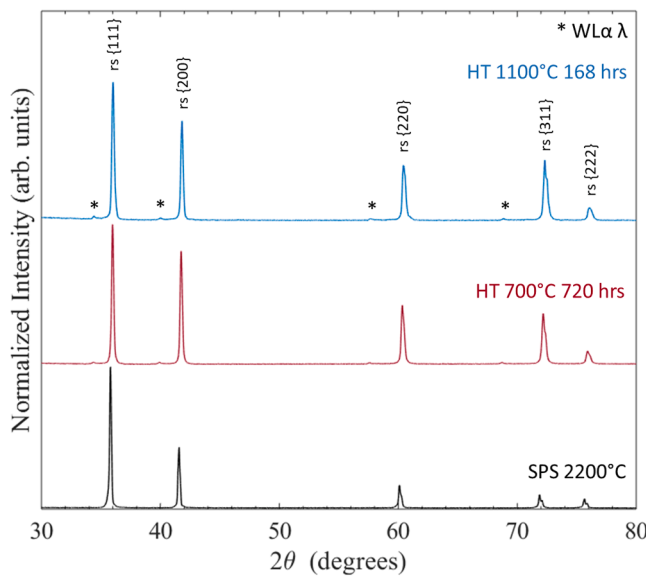


Fig. 8. XRD patterns from a sample of MoNbTaVWC_5 after high temperature sintering at 2200°C (bottom), heat treatment at 700°C for 720 h (middle), and heat treatment at 1100°C for 168 h (top). Note that only the single-phase rocksalt (rs) structure is maintained after all heat treatments.

H_V of 14.6 ± 1.4 GPa and a K_{ifr} of 3.6 ± 0.3 MPa $\cdot m^{\frac{1}{2}}$ as measured in this study (H_V of ~ 12 – 16 GPa and K_{ifr} of 2 – 20 MPa $\cdot m^{\frac{1}{2}}$ in literature [24,76]). The compositions CrMoNbVWC_5 and CrMoTaVWC_5 maintain a hardness of ~ 23.3 GPa, on par with the low-VEC materials studied herein, while achieving a K_{ifr} of 4.2 ± 0.4 MPa $\cdot m^{\frac{1}{2}}$ and 4.9 ± 0.3 MPa $\cdot m^{\frac{1}{2}}$, respectively. Thus, through Fermi energy engineering, high-entropy carbides have demonstrated a combination of high hardness and fracture resistance that is rarely achieved in materials. This theory lays the groundwork for the use of chemistry selection in high-entropy ceramics to produce high hardness and ultra-tough rocksalt carbide, nitride, and carbonitride materials, that were previously unattainable. The compositional choice of high-entropy materials greatly affect their electronic density of states. In the case of metal carbides, tailoring iDOS(E_{pg} , E_F) results in improved mechanical properties.

5. Conclusion

High-entropy carbides are shown to increase in ductility with VEC and iDOS(E_{pg} , E_F). The iDOS(E_{pg} , E_F) parameter is demonstrated to better correlate with the moduli, Pugh's criteria and Cauchy pressure than DOS or VEC. Loosely analogous to what is done in semiconductors, Fermi-level engineering is determined to be an effective method for predicting and engineering the metallic character of bonding resulting in improved mechanical properties. The indentation fracture resistance measurements support the computational results, showing increased metallicity of the bonding beyond what is achievable in binary and ternary B1 carbides yielding significant improvement in a carbide's ability to accommodate plastic flow. This conclusion is further supported by the excellent correlation with the trends observed in the effective fracture resistance data. The examples of MoNbTaVWC_5 , CrMoNbVWC_5 and CrMoTaVWC_5 showing that entropy can enable high VEC and iDOS(E_{pg} , E_F) in a cubic structure, highlights a new path for tailoring mechanical properties. Given the wide range of composition space the premise of high-entropy materials has unlocked, it is expected that there exists significant opportunity to leverage this computational design strategy to find compositions with a further enhanced combination of properties. There is expected to be particular interest in increasing the iDOS(E_{pg} , E_F), likely via further concentration of Cr, Mo,

or W, in high-entropy carbide, nitride, and carbonitride compositions.

Data availability

All *ab initio* data are publicly available through the AFLOW online repository (aflow.org) and can be accessed using the REST-API interface [77] and the AFLUX search-API [78].

CRediT authorship contribution statement

Kenneth Vecchio: Conceptualization, Funding acquisition, Investigation, Methodology, Project administration, Resources, Supervision, Writing – review & editing. **Stefano Curtarolo:** Formal analysis, Funding acquisition, Methodology, Project administration, Supervision, Validation, Writing – review & editing. **Kevin Kaufmann:** Formal analysis, Validation, Writing – review & editing. **Tyler J. Harrington:** Formal analysis, Investigation, Methodology, Validation, Writing – original draft. **Corey Oses:** Data curation, Software, Validation. **Cormac Toher:** Data curation, Investigation, Methodology, Software, Validation, Writing – review & editing.

Declaration of competing interest

The authors declare that they have no competing financial interests or personal relationships that could have appeared to influence the work reported in this paper.

Acknowledgements

The authors acknowledge support by DOD-ONR (N00014-15-1-2863, N00014-17-1-2090, N00014-16-1-2583, N00014-17-1-2876) and by Duke University—Center for Extreme Materials—for computational support. K. Kaufmann was supported by the Department of Defense (DoD) through the National Defense Science and Engineering Graduate Fellowship (NDSEG) Program. K. Kaufmann would also like to acknowledge the support of the ARCS Foundation, San Diego Chapter. K. Vecchio would like to acknowledge the financial generosity of the Oerlikon Group in support of his research group. The authors would like to thank Dr. Jaskaran Saini for assistance with fabricating and collecting K_{ifr} data for several of the samples. The authors would also like to thank Dr. Sicong Jiang for assistance with DFT modeling.

References

- [1] E. Wuchina, E. Opila, M. Opeka, W. Fahrenholtz, I. Talmy, UHTCs: ultra-high temperature ceramic materials for extreme environment applications, *Electrochim. Soc. Interface.* 16 (2007).
- [2] L.E. Toth, *Transition Metal Carbides and Nitrides*, Academic Press, New York, 1971.
- [3] W.R. Slivka, Gas tungsten and plasma arc welding electrode having a carbide emitter end, 5124528, 1992.
- [4] D. Edström, D.G. Sangiovanni, L. Hultman, I. Petrov, J.E. Greene, V. Chirita, Elastic properties and plastic deformation of TiC- and VC-based pseudobinary alloys, *Acta Mater.* 144 (2018) 376–385, <https://doi.org/10.1016/j.actamat.2017.10.047>.
- [5] H.W. Hugosson, U. Jansson, B. Johansson, O. Eriksson, Restricting dislocation movement in transition metal carbides by phase stability tuning, *Science* (80-). 293 (2001) 2434–2437. [doi:10.1126/science.1060512](https://doi.org/10.1126/science.1060512).
- [6] J. Hu, Q. Yang, S. Zhu, Y. Zhang, D. Yan, K. Gan, Z. Li, Superhard bulk high-entropy carbides with enhanced toughness via metastable in-situ particles, *Nat. Commun.* 14 (14) (2023) 1–12, <https://doi.org/10.1038/s41467-023-41481-6>, 2023.
- [7] D.C. Hofmann, J.-Y. Suh, A. Wiest, G. Duan, M.-L. Lind, M.D. Demetriou, W. L. Johnson, Designing metallic glass matrix composites with high toughness and tensile ductility, *Nature* 451 (2008) 1085–1089, <https://doi.org/10.1038/nature06598>.
- [8] F.F. Lange, Transformation toughening, *J. Mater. Sci.* 17 (1982) 247–254, <https://doi.org/10.1007/BF00809060>.
- [9] O. Malek, B. Lauwers, Y. Perez, P. De Baets, J. Vleugels, Processing of ultrafine ZrO₂ toughened WC composites, *J. Eur. Ceram. Soc.* 29 (2009) 3371–3378, <https://doi.org/10.1016/J.JEURCERAMSOC.2009.07.013>.

- [10] W. Jiang, H. Lu, J. Chen, X. Liu, C. Liu, X. Song, Toughening cemented carbides by phase transformation of zirconia, *Mater. Des.* 202 (2021) 109559, <https://doi.org/10.1016/J.MATDES.2021.109559>.
- [11] A.G. Evans, R.M. Cannon, Toughening of brittle solids by martensitic transformations, *Acta Met. (United States)*. 34 (5) (1986) 761–800, [https://doi.org/10.1016/0001-6160\(86\)90052-0](https://doi.org/10.1016/0001-6160(86)90052-0).
- [12] N. De Leon, X.X. Yu, H. Yu, C.R. Weinberger, G.B. Thompson, Bonding effects on the slip differences in the B1 monocarbides, *Phys. Rev. Lett.* 114 (2015), <https://doi.org/10.1103/PhysRevLett.114.165502>.
- [13] C.J. Smith, X.X. Yu, Q. Guo, C.R. Weinberger, G.B. Thompson, Phase, hardness, and deformation slip behavior in mixed $Hf_xTa_{1-x}C$, *Acta Mater.* 145 (2018) 142–153, <https://doi.org/10.1016/j.actamat.2017.11.038>.
- [14] L. Pizzagalli, P. Beauchamp, First principles determination of the Peierls stress of the shuffle screw dislocation in silicon, *Philos. Mag. Lett.* 84 (2004) 729–736, <https://doi.org/10.1080/09500830500041377>.
- [15] Y. Wang, T. Csanádi, H. Zhang, J. Dusza, M.J. Reece, R. Zhang, Enhanced Hardness in High-Entropy Carbides through Atomic Randomness, *Adv. Theory Simulations*. 3 (2020) 2000111, <https://doi.org/10.1002/adts.202000111>.
- [16] S.H. Jhi, J. Ihm, S.G. Louie, M.L. Cohen, Electronic mechanism of hardness enhancement in transition-metal carbonitrides, *Nature* 399 (1999) 132–134, <https://doi.org/10.1038/00141948>.
- [17] A. Kelly, *Strong Solids*, Clarendon Press, Oxford, 1986.
- [18] J.A. Wollmershauser, B.N. Feigelson, E.P. Gorzkowski, C.T. Ellis, R. Goswami, S. B. Qadri, J.G. Tischler, F.J. Kub, R.K. Everett, An extended hardness limit in bulk nanoceramics, *Acta Mater.* 69 (2014) 9–16, <https://doi.org/10.1016/j.actamat.2014.01.030>.
- [19] A.H. Heuer, G.K. Bansal, Precipitation Hardening in Ceramics (Eds.), in: M. S. Seltzer, R.I. Jaffee (Eds.), *Defects Transp. Oxides*, 1974, pp. 415–423, https://doi.org/10.1007/978-1-4615-8723-1_23.
- [20] E.A. Levashov, V.V. Kurbatkina, A.A. Zaitsev, S.I. Rupasov, E.I. Patsera, A. A. Chernyshev, Y.V. Zubavichus, A.A. Velizhanin, Structure and properties of precipitation-hardening ceramic Ti-Zr-C and Ti-Ta-C materials, *Phys. Met. Met. 109* (2010) 95–105, <https://doi.org/10.1134/S0031918x10010102>.
- [21] C. Oses, C. Toher, S. Curtarolo, High-entropy ceramics, *Nat. Rev. Mater.* (2020) 1–15, <https://doi.org/10.1038/s41578-019-0170-8>.
- [22] X.-X. Yu, G.B. Thompson, C.R. Weinberger, Influence of carbon vacancy formation on the elastic constants and hardening mechanisms in transition metal carbides, *J. Eur. Ceram. Soc.* 35 (2015) 95–103, <https://doi.org/10.1016/j.jeurceramsoc.2014.08.021>.
- [23] K. Kaufmann, E. Wenger, K. Vecchio, Synthesis and evaluation of rocksalt structure (Mo, W) carbides via vanadium additions, *Scr. Mater.* 229 (2023) 115382, <https://doi.org/10.1016/J.SCRIPTAMAT.2023.115382>.
- [24] D.J. Rowcliffe, G.E. Hollox, Plastic flow and fracture of tantalum carbide and hafnium carbide at low temperatures, *J. Mater. Sci.* 6 (1971) 1261–1269, <https://doi.org/10.1007/BF00552039>.
- [25] S.-H. Jhi, S.G. Louie, M.L. Cohen, J.W. Morris, Mechanical instability and ideal shear strength of transition metal carbides and nitrides, *Phys. Rev. Lett.* 87 (2001) 075503, <https://doi.org/10.1103/PhysRevLett.87.075503>.
- [26] A. Nieto, D. Lahiri, A. Agarwal, Graphene NanoPlatelets reinforced tantalum carbide consolidated by spark plasma sintering, *Mater. Sci. Eng. A* 582 (2013) 338–346, <https://doi.org/10.1016/J.MSEA.2013.06.006>.
- [27] K. Balasubramanian, S.V. Khare, D. Gall, Valence electron concentration as an indicator for mechanical properties in rocksalt structure nitrides, carbides and carbonitrides, *Acta Mater.* 152 (2018) 175–185, <https://doi.org/10.1016/j.actamat.2018.04.033>.
- [28] D.G. Sangiovanni, L. Hultman, V. Chirita, Supertoughening in B1 transition metal nitride alloys by increased valence electron concentration, *Acta Mater.* 59 (2011) 2121–2134, <https://doi.org/10.1016/j.actamat.2010.12.013>.
- [29] H. Yu, M. Bahadori, G.B. Thompson, C.R. Weinberger, Understanding dislocation slip in stoichiometric rocksalt transition metal carbides and nitrides, *J. Mater. Sci.* 52 (2017) 6235–6248, <https://doi.org/10.1007/s10853-017-0857-4>.
- [30] D.G. Sangiovanni, V. Chirita, L. Hultman, Electronic mechanism for toughness enhancement in Ti_xM_1-xN ($M=Mo$ and W), *Phys. Rev. B* 81 (2010) 104107, <https://doi.org/10.1103/PhysRevB.81.104107>.
- [31] T. Joelsson, L. Hultman, H.W. Hugosson, J.M. Molina-Aldareguia, Phase stability tuning in the $NbxZr_{1-x}N$ thin-film system for large stacking fault density and enhanced mechanical strength, *Appl. Phys. Lett.* 86 (2005) 131922, <https://doi.org/10.1063/1.1884743>.
- [32] D.G. Sangiovanni, L. Hultman, V. Chirita, I. Petrov, J.E. Greene, Effects of phase stability, lattice ordering, and electron density on plastic deformation in cubic $TiWN$ pseudobinary transition-metal nitride alloys, *Acta Mater.* 103 (2016) 823–835, <https://doi.org/10.1016/j.actamat.2015.10.039>.
- [33] D.G. Sangiovanni, K. Kaufmann, K. Vecchio, Valence electron concentration as key parameter to control the fracture resistance of refractory high-entropy carbides, *Sci. Adv.* 9 (2023), <https://doi.org/10.1126/sciadv.adz2960>.
- [34] D.G. Sangiovanni, W. Mellor, T. Harrington, K. Kaufmann, K. Vecchio, Enhancing plasticity in high-entropy refractory ceramics via tailoring valence electron concentration, *Mater. Des.* 209 (2021) 109932, <https://doi.org/10.1016/J.MATDES.2021.109932>.
- [35] H. Kindlund, D.G. Sangiovanni, J. Lu, J. Jensen, V. Chirita, J. Birch, I. Petrov, J. E. Greene, L. Hultman, Vacancy-induced toughening in hard single-crystal $V_{0.5}Mo_{0.5}N_x/MgO(0\ 0)$ thin films, *Acta Mater.* 77 (2014) 394–400, <https://doi.org/10.1016/j.actamat.2014.06.025>.
- [36] H. Holleck, Material selection for hard coatings, *J. Vac. Sci. Technol. A Vacuum, Surfaces, Film.* 4 (1986) 2661–2669, <https://doi.org/10.1116/1.573700>.
- [37] S.H. Jhi, S.G. Louie, M.L. Cohen, J. Ihm, Vacancy hardening and softening in transition metal carbides and nitrides, *Phys. Rev. Lett.* 86 (2001) 3348–3351, <https://doi.org/10.1103/PhysRevLett.86.3348>.
- [38] D. Edström, D.G. Sangiovanni, L. Hultman, V. Chirita, Effects of atomic ordering on the elastic properties of TiN- and VN-based ternary alloys, *Thin Solid Films* 571 (2014) 145–153, <https://doi.org/10.1016/j.tsf.2014.09.048>.
- [39] F. Tian, J. D'Arcy-Gall, T.-Y. Lee, M. Sardela, D. Gall, I. Petrov, J.E. Greene, Epitaxial $Ti_{1-x}W_xN$ alloys grown on $MgO(001)$ by ultrahigh vacuum reactive magnetron sputtering: electronic properties and long-range cation ordering, *J. Vac. Sci. Technol. A* 21 (2003) 140–146, <https://doi.org/10.1116/1.1525818>.
- [40] H. Kindlund, J. Lu, J. Jensen, I. Petrov, J.E. Greene, L. Hultman, Epitaxial $V_{0.6}W_{0.4}N/MgO(001)$: evidence for ordering on the cation sublattice, *J. Vac. Sci. Technol. A* 31 (2013) 040602, <https://doi.org/10.1116/1.4807654>.
- [41] H. Kindlund, D.G. Sangiovanni, L. Martínez-De-Olcoz, J. Lu, J. Jensen, J. Birch, I. Petrov, J.E. Greene, V. Chirita, L. Hultman, Toughness enhancement in hard ceramic thin films by alloy design, *APL Mater.* 1 (2013) 042104, <https://doi.org/10.1063/1.4822440>.
- [42] D.G. Sangiovanni, Inherent toughness and fracture mechanisms of refractory transition-metal nitrides via density-functional molecular dynamics, *Acta Mater.* 151 (2018) 11–20, <https://doi.org/10.1016/j.actamat.2018.03.038>.
- [43] D. Holec, M. Friák, J. Neugebauer, P.H. Mayrhofer, Trends in the elastic response of binary early transition metal nitrides, *Phys. Rev. B* 85 (2012) 064101, <https://doi.org/10.1103/PhysRevB.85.064101>.
- [44] T. Das, S. Deb, A. Moorkjee, Study of electronic structure and elastic properties of transition metal and actinide carbides, *Phys. B Condens. Matter.* 367 (2005) 6–18, <https://doi.org/10.1016/j.physb.2005.05.041>.
- [45] A. Pasturel, C. Colinet, P. Hicter, Strong chemical interactions in disordered alloys, *Phys. B+C* 132 (1985) 177–180, [https://doi.org/10.1016/0378-4363\(85\)90062-2](https://doi.org/10.1016/0378-4363(85)90062-2).
- [46] E.I. Isaev, S.I. Simak, I.A. Abrikosov, R. Ahuja, Y.K. Vekilov, M.I. Katsnelson, A. I. Lichtenstein, B. Johansson, Phonon related properties of transition metals, their carbides, and nitrides: a first-principles study, *J. Appl. Phys.* 101 (2007) 123519, <https://doi.org/10.1063/1.2747230>.
- [47] P. Řehák, M. Černý, D. Holec, Interface-induced electronic structure toughening of nitride superlattices, *Surf Coat Technol* 325 (2017) 410–416, <https://doi.org/10.1016/j.surcoat.2017.06.065>.
- [48] F. Kubel, W. Lengauer, K. Yvon, K. Knorr, A. Junod, Structural phase transition at 205 K in stoichiometric vanadium nitride, *Phys. Rev. B* 38 (1988) 12908–12912, <https://doi.org/10.1103/PhysRevB.38.12908>.
- [49] A.B. Mei, O. Hellman, N. Wireklint, C.M. Schlepütz, D.G. Sangiovanni, B. Alling, A. Rockett, L. Hultman, I. Petrov, J.E. Greene, Dynamic and structural stability of cubic vanadium nitride, *Phys. Rev. B* 91 (2015) 054101, <https://doi.org/10.1103/PhysRevB.91.054101>.
- [50] S. Hu, C. Xu, Y. Lao, Y. Wang, H. Zhang, G.J. Zhang, J. Yang, The stabilization of the rocksalt structured tantalum nitride, *J. Appl. Phys.* 122 (2017) 045109, <https://doi.org/10.1063/1.4989415>.
- [51] D.G. Sangiovanni, Mass transport properties of quasiharmonic vs. anharmonic transition-metal nitrides, *Thin Solid Films* 688 (2019) 137297, <https://doi.org/10.1016/j.tsf.2019.05.016>.
- [52] T.J. Harrington, J. Gild, P. Sarker, C. Toher, C.M. Rost, O.F. Dippo, C. McElfresh, K. Kaufmann, E. Marin, L. Borowski, P.E. Hopkins, J. Luo, S. Curtarolo, D. W. Brenner, K.S. Vecchio, Phase stability and mechanical properties of novel high entropy transition metal carbides, *Acta Mater.* 166 (2019) 271–280, <https://doi.org/10.1016/j.actamat.2018.12.054>.
- [53] P. Sarker, T. Harrington, C. Toher, C. Oses, M. Samiee, J.P. Maria, D.W. Brenner, K. S. Vecchio, S. Curtarolo, High-entropy high-hardness metal carbides discovered by entropy descriptors, *Nat. Commun.* 9 (2018) 4980, <https://doi.org/10.1038/s41467-018-07160-7>.
- [54] K. Kaufmann, D. Maryanovsky, W.M. Mellor, C. Zhu, A.S. Rosengarten, T. J. Harrington, C. Oses, C. Toher, S. Curtarolo, K.S. Vecchio, Discovery of high-entropy ceramics via machine learning, *Npj Comput. Mater.* 6 (2020) 42, <https://doi.org/10.1038/s41524-020-0317-6>.
- [55] W.M. Mellor, K. Kaufmann, O.F. Dippo, S.D. Figueroa, G.D. Schrader, K.S. Vecchio, Development of ultrahigh-entropy ceramics with tailored oxidation behavior, *J. Eur. Ceram. Soc.* 41 (2021) 5791–5800, <https://doi.org/10.1016/J.JEURCERAMSC.2021.05.010>.
- [56] K. Yang, C. Oses, S. Curtarolo, Modeling Off-Stoichiometry Materials with a High-Throughput Ab-Initio Approach, *Chem. Mater.* 28 (2016) 6484–6492, <https://doi.org/10.1021/acs.chemmater.6b01449>.
- [57] C. Oses, C. Toher, S. Curtarolo, Data-driven design of inorganic materials with the Automatic Flow Framework for Materials Discovery, *MRS Bull.* 43 (2018) 670–675, <https://doi.org/10.1557/mrs.2018.207>.
- [58] C. Toher, C. Oses, D. Hicks, E. Gossett, F. Rose, P. Nath, D. Usanmaz, D.C. Ford, E. Perim, C.E. Calderon, J.J. Plata, Y. Lederer, M. Jahnátek, W. Setyawati, S. Wang, J. Xue, K. Rasch, R.V. Chepulkii, R.H. Taylor, G. Gomez, H. Shi, A.R. Supka, R.A. R. Al Orabi, P. Gopal, F.T. Cerasoli, L. Liyanage, H. Wang, I. Siloi, L.A. Agapito, C. Nyshadham, G.L.W. Hart, J. Carrete, F. Legrain, N. Mingo, E. Zurek, O. Isayev, A. Tropsha, S. Sanvitto, R.M. Hanson, I. Takeuchi, M.J. Mehl, A.N. Kolmogorov, K. Yang, P. D'Amico, A. Calzolari, M. Costa, R. De Gennaro, M.B. Nardelli, M. Fornari, O. Levy, S. Curtarolo, The AFLW Fleet for Materials Discovery. Handb. Mater. Model, Springer International Publishing, Cham, 2018, pp. 1–28, https://doi.org/10.1007/978-3-319-42913-7_63-1.
- [59] A.K. Rappe, C.J. Casewell, K.S. Colwell, W.A. Goddard III, W.M. Skiff, UFF, a full periodic table force field for molecular mechanics and molecular dynamics simulations, *J. Am. Chem. Soc.* 114 (1992) 10024–10035, <https://doi.org/10.1021/ja00051a040>.

- [60] M.J. Mehl, D. Hicks, C. Toher, O. Levy, R.M. Hanson, G. Hart, S. Curtarolo, The AFLOW Library of Crystallographic Prototypes: part 1, Comput. Mater. Sci. 136 (2017) S1–S828, <https://doi.org/10.1016/j.commatsci.2017.01.017>. Suppl.
- [61] C.E. Calderon, J.J. Plata, C. Toher, C. Oses, O. Levy, M. Fornari, A. Natan, M. J. Mehl, G. Hart, M. Buongiorno Nardelli, S. Curtarolo, The AFLOW standard for high-throughput materials science calculations, Comput. Mater. Sci. 108 (2015) 233–238, <https://doi.org/10.1016/J.COMMATSCL.2015.07.019>.
- [62] C.M. Rost, Z. Rak, D.W. Brenner, J.-P. Maria, Local structure of the $MgxNixCoxCuxZnxO(x=0.2)$ entropy-stabilized oxide: an EXAFS study, J. Am. Ceram. Soc. 100 (2017) 2732–2738, <https://doi.org/10.1111/jace.14756>.
- [63] C. Toher, C. Oses, J.J. Plata, D. Hicks, F. Rose, O. Levy, M. de Jong, M. Asta, M. Fornari, M. Buongiorno Nardelli, S. Curtarolo, Combining the AFLOW GIBBS and elastic libraries to efficiently and robustly screen thermomechanical properties of solids, Phys. Rev. Mater. 1 (2017) 015401, <https://doi.org/10.1103/PhysRevMaterials.1.015401>.
- [64] F. Tasnádi, M. Odén, I.A. Abrikosov, *Ab initio* elastic tensor of cubic $Ti_{0.5}Al_{0.5}N$ alloys: dependence of elastic constants on size and shape of the supercell model and their convergence, Phys. Rev. B. 85 (2012) 144112, <https://doi.org/10.1103/PhysRevB.85.144112>.
- [65] X.Q. Chen, H. Niu, D. Li, Y. Li, Modeling hardness of polycrystalline materials and bulk metallic glasses, Intermetallics 19 (2011) 1275–1281, <https://doi.org/10.1016/j.intermet.2011.03.026>.
- [66] D.M. Teter, Computational alchemy: the search for new superhard materials, MRS Bull. 23 (1998) 22–27, <https://doi.org/10.1557/S0883769400031420>.
- [67] Y. Tian, B. Xu, Z. Zhao, Microscopic theory of hardness and design of novel superhard crystals, Int. J. Refract. Met. Hard Mater. 33 (2012) 93–106, <https://doi.org/10.1016/J.IJRMHM.2012.02.021>.
- [68] P. Avery, X. Wang, C. Oses, E. Gossett, D.M. Proserpio, C. Toher, S. Curtarolo, E. Zurek, Predicting superhard materials via a machine learning informed evolutionary structure search, Npj Comput. Mater. 5 (2019) 1–11, <https://doi.org/10.1038/s41524-019-0226-8>.
- [69] D. Edström, D.G. Sangiovanni, L. Landälv, P. Eklund, J.E. Greene, I. Petrov, L. Hultman, V. Chirita, Mechanical properties of VMoNO as a function of oxygen concentration: toward development of hard and tough refractory oxynitrides, J. Vac. Sci. Technol. A. 37 (2019) 061508, <https://doi.org/10.1116/1.5125302>.
- [70] G.R. Anstis, P. Chantikul, B.R. Lawn, D.B. Marshall, A Critical Evaluation of Indentation Techniques for Measuring Fracture Toughness: I, Direct Crack Measurements, J. Am. Ceram. Soc. 64 (1981) 533–538, <https://doi.org/10.1111/j.1151-2916.1981.tb10320.x>.
- [71] S.F. Pugh, XCII, Relations between the elastic moduli and the plastic properties of polycrystalline pure metals, Lond. Edinb. Dubl. Phil. Mag. 45 (1954) 823–843, <https://doi.org/10.1080/14786440808520496>.
- [72] K. Chen, L.R. Zhao, J. Rodgers, J.S. Tse, Alloying effects on elastic properties of TiN-based nitrides, J. Phys. D Appl. Phys. 36 (2003) 2725–2729, <https://doi.org/10.1088/0022-3727/36/21/021>.
- [73] D.G. Pettifor, Theoretical predictions of structure and related properties of intermetallics, Mater. Sci. Technol. 8 (1992) 345–349, <https://doi.org/10.1179/mst.1992.8.4.345>.
- [74] R.A. Johnson, Analytic nearest-neighbor model for fcc metals, Phys. Rev. B. 37 (1988) 3924–3931, <https://doi.org/10.1103/PhysRevB.37.3924>.
- [75] A.J. Schwartz, M. Kumar, B.L. Adams, D.P. Field, Electron Backscatter Diffraction in Materials Science, Springer Science+Business Media, LLC, New York, 2009, <https://doi.org/10.1007/978-0-387-88136-2>.
- [76] W. Fahrenholtz, Ultra-high temperature ceramics : materials for extreme environment applications, n.d.
- [77] R.H. Taylor, F. Rose, C. Toher, O. Levy, K. Yang, M. Buongiorno Nardelli, S. Curtarolo, A RESTful API for exchanging materials data in the AFLOWLIB.org consortium, Comput. Mater. Sci. 93 (2014) 178–192, <https://doi.org/10.1016/j.commatsci.2014.05.014>.
- [78] F. Rose, C. Toher, E. Gossett, C. Oses, M. Buongiorno Nardelli, M. Fornari, S. Curtarolo, Editor's Choice AFLUX: the LUX materials search API for the AFLOW data repositories, (2017). doi:[10.1016/j.commatsci.2017.04.036](https://doi.org/10.1016/j.commatsci.2017.04.036).
- [79] C. Toher, C. Oses, D. Hicks, S. Curtarolo, Unavoidable disorder and entropy in multi-component systems, npj Comput. Mater. 5 (2019) 69, <https://doi.org/10.1038/s41524-019-0206-z>.
- [80] S. Divilov, H. Eckert, D. Hicks, C. Oses, C. Toher, R. Friedrich, M. Esters, M.J. Mehl, A.C. Zettel, Y. Lederer, E. Zurek, J.-P. Maria, D.W. Brenner, X. Campilongo, S. Filipovic, W.G. Fahrenholtz, C.J. Ryan, C.M. DeSalle, R.J. Crealese, D.E. Wolfe, A. Calzolari, S. Curtarolo, Disordered enthalpy-entropy descriptor for high-entropy ceramics discovery, Nature 625 (2024) 66–73, <https://doi.org/10.1038/s41586-023-06786-y>.